Vacuum 84 (2010) 817–822

Contents lists available at ScienceDirect

Vacuum

journal homepage: www.elsevier.com/locate/vacuum

Characterization and properties of TiN-containing amorphous Ti–Si–N nanocomposite coatings prepared by arc assisted middle frequency magnetron sputtering

C.W. Zou, H.J. Wang, M. Li, Y.F. Yu, C.S. Liu, L.P. Guo, D.J. Fu*

Accelerator Laboratory, Department of Physics and Key Laboratory of Acoustic and Photonic Materials and Devices of Ministry of Education, Wuhan University, Wuhan 430072, China

ARTICLE INFO

Article history:
Received 20 August 2009
Received in revised form
23 October 2009
Accepted 31 October 2009

Keywords:
Ti–Si–N nanocomposite coatings
Middle frequency magnetron sputtering
Friction coefficient
Hardness

ABSTRACT

TiN-containing amorphous Ti–Si–N (nc-TiN/a-Si_3N_4) nanocomposite coatings were deposited by using a modified closed field unbalanced middle frequency magnetron sputtering system which is arc assisted and consists of two circles of targets, at a substrate temperature of 400 °C. The coatings exhibit good mechanical properties that are greatly influenced by the total gas pressure and N_2/Ar ratios. For coatings prepared at a N_2/Ar ratio of 3:1, the hardness increases from 24 GPa at a total gas pressure of 0.2 Pa–58 GPa at 0.4 Pa, and then, the hardness decreases gradually when the total gas pressure was further increased. On the other hand, the friction coefficient decreases monotonously with increasing total gas pressure. XRD, XPS and high resolution TEM experiments showed that the coatings contain TiN nanocrystals embedded in the amorphous Si_3N_4 matrix. The coating deposited under optimum conditions exhibits excellent tribological performance with a low friction coefficient of 0.42 and a high hardness of 58 GPa. These properties make it possible for industrial applications.

1. Introduction

Ti–Si–N coatings have been investigated for many years for their outstanding mechanical properties such as high hardness, low wear coefficient, and high chemical stability [1–5]. However, due to the use of toxic gas for metal sources and high substrate temperature in chemical vapor deposition (CVD), physical vapor deposition (PVD) technique is considered to be more suitable for industrial-scale synthesis of these coatings. The main PVD methods are cathode arc and magnetron sputtering. The cathodic-arc deposition technique possesses good adhesion and higher deposition rate due to its high ionization and high current density [6]. However, it has emission of micrometer sized droplets of cathode material from the arc spots, commonly referred to as macroparticles. For magnetron sputtering, Ti–Si–N coatings are generally prepared by using closed field unbalanced magnetron sputtering systems by simultaneous sputtering of Ti and Si targets [7,8]. However, due to the low ionization of magnetron sputtering, when such systems were used to coat work pieces with complicated geometry, the stability of the sputtering process, the adhesion and uniformity of the coatings as well as the reproducibility are not satisfactory.

To realize large scale deposition with high uniformity of Ti–Si–N coatings on random-shape machining tools and moulds, it is necessary to maintain a high plasma density in the deposition chamber. In this article, we present a design of a modified middle frequency magnetron (MF) sputtering system and properties of Ti–Si–N coatings deposited by using this system.

2. Experimental details

The Ti–Si–N nanocomposite coatings were deposited by using a modified closed field unbalanced magnetron sputtering system which is arc assisted and consists of two circles of targets, with a dimension of $\Phi 1000 \times 1000$ mm^2, as shown in Fig. 1. The opposed target configuration consists of eight targets; four of them are placed vertically on the sidewalls of the deposition chamber and the remaining four inner targets were placed around the center of the chamber. The magnets of these four pair targets were placed behind the targets with magnetic poles opposing to each other to form the closed magnetic fields. Furthermore, the magnet arrangement of the four outer targets forms a closed magnetic field and the four inner targets form a closed magnetic field. In such magnetic field configuration the plasma is tightly confined between the four paired targets, resulting in a high plasma density in the

* Corresponding author. Tel./fax: +86 27 6875 3587.
E-mail address: changweizou@hotmail.com (D.J. Fu).

0042-207X/$ – see front matter © 2009 Elsevier Ltd. All rights reserved.
doi:10.1016/j.vacuum.2009.10.050

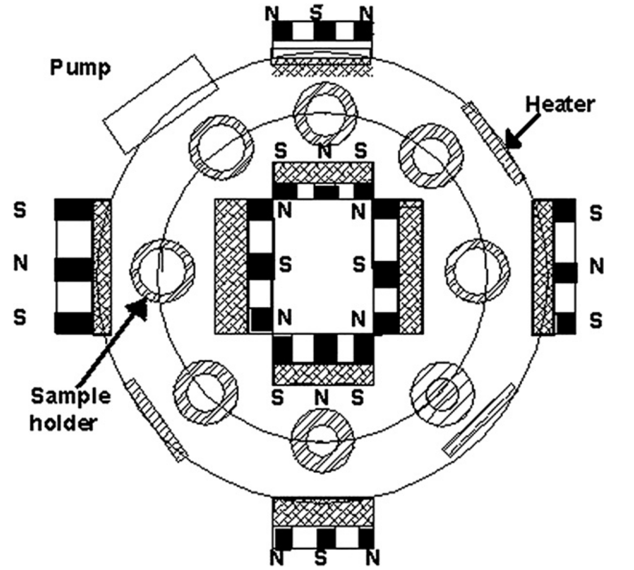

Fig. 1. Schematic cross-sectional view of the cathodic-arc assisted closed field unbalanced middle frequency magnetron sputtering system.

chamber. To improve the adhesion, a twin-purpose Ti cathode was designed, which either can be run in arc or magnetron sputtering mode. The substrates were placed vertically on a rotating sample carrier which was in between the pair targets. The targets were powered with bipolar 40 kHz power supplies. The samples spun in addition to rotation, and the base pressure prior to coating deposition was 8×10^{-4} Pa. During deposition, the substrates rotated in the deposition chamber and faced two pair of Ti targets (99.99%) and two pair of Si targets (99.99%) sequentially. The pulsed substrate bias was fixed at 150 V to optimize the deposition condition and the output current of Ti paired targets was fixed at 120 A, while the output power to the Si paired targets was fixed at 20 A. The mirror-polished stainless steel and Si (111) wafers were used as substrates and the coating process consisted of a 15-min deposition of a pure Ti layer and a 60-min deposition of Ti–Si–N layer. Typical deposition conditions for Ti–Si–N coatings were shown in Table 1. N_2/Ar ratio or total gas pressure was varied at a time and then the changes in the resulting coatings were investigated.

The crystal structure of the coatings was characterized by X-ray diffraction (XRD, D8ADVACE) with Cu Kα radiation. The surface morphologies of the Ti–Si–N coatings were measured on a SHIMADZU SPM-9500J3 atomic force microscope (AFM). The Ti elemental concentration was determined by using an EDAX genesis 7000 energy dispersive spectrometer (EDS) system operated at 25 kV. The chemical bonding was investigated by a Kratos 2AXIS2HS X-ray photoelectron spectroscopy (XPS) system using Mg Kα (1253.6 eV) radiation. The microstructure measurements of coatings were carried out on JEM-2010FEF (UHR) transmission electron microscopes (TEM) operated at 200 kV. The hardness of the coatings was measured with a fully calibrated MTS Nano Indenter XP. The depth of indentation was set at 200 nm to avoid surface and substrate effect. On each sample, ten indentations were made at random locations and ten hardness values calculated for an average. During the tests the samples were given a maximum load (L_{max}) and held there for 10 s. Thereafter they unload with 10% of the L_{max} and held for 30 s. The test ended with a second maximum loading (L_{max}) and a 10 s hold, after which a complete unloading took place. An MS-T3000 ball-on-disc tester was used for the friction and wear measurements of the Ti–Si–N coatings, which slide in ambient air at 23 °C and relative humidity (RH) 60%; a WC-Co ball with 6 mm in diameter was used as the mating material. A 5 N load was applied on the ball. The average sliding speed was 0.02 m/s for a fixed sliding time of 100 min and the friction coefficients of the coatings were continuously recorded during the test.

Table 1
Typical conditions for Ti–Si–N nanocomposite coatings deposited by cathodic-arc assisted middle frequency magnetron sputtering system.

Parameters	Values
Working pressure (Pa)	0.4
N2 flow rate (sccm)	150
Ar flow rate (sccm)	50
Ti arc targets current (A)	120
Si magnetron current	20
Substrate temperature (°C)	400
Negative bias voltage (V)	150

3. Results and discussions

Fig. 2 shows the XRD patterns for Ti–Si–N coatings deposited at various total gas pressures. It was found that all the Ti–Si–N coatings had a polycrystalline structure with multiple crystal planes orientations of TiN (111), (200), (220), (311) and (222), respectively. The primary (111) diffraction peaks broadened obviously with increasing total gas pressures.

Fig. 3 shows the XRD patterns for Ti–Si–N coatings deposited at various N_2/Ar ratios. It was demonstrated that all the deposited coatings possessed a preferred orientation of (111) and this (111) peak broadened with increasing N_2/Ar ratios. This peak broadening behavior was usually originated from the diminution of grain size [9] and the existence of residual stress induced in the crystal lattice [10]. No diffraction peaks assigned to Si_3N_4 or other titanium silicon phases was observed and it was suggested that silicon may exist as an amorphous silicon nitride phase. The TiN crystallite sizes were calculated from (111) diffraction patterns using Scherrer formula by assuming the shape factor of 1 [11] and the results are shown in Fig. 4. TiN crystallite sizes decreased from about 11 to 8 nm when the N_2/Ar ratio was increased from 1:2 to 3:1. However, the TiN size re-increased to 9.3 nm when the N_2/Ar ratio was further increased to 4:1. The minimum TiN crystallize size was obtained at N_2/Ar ratio of 3. Meanwhile, as can be seen from Fig. 4b, the TiN size decreased from 14 to 8 nm when the total gas pressure was increased from 0.2 to 0.4 Pa, and then, it re-increased gradually to ∼10 nm when the total gas was further increased. Fig. 4c shows the N, Ti, and Si contents in Ti–Si–N films as a function of N_2/Ar ratios at a fixed total gas pressure of 0.4 Pa. The N contents in Ti–Si–N coatings

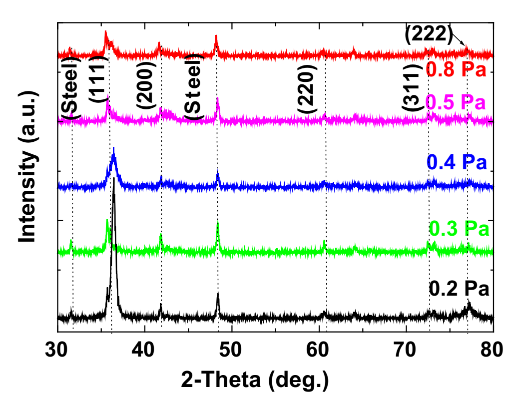

Fig. 2. XRD patterns for Ti–Si–N nanocomposite coatings deposited under various total gas pressures.

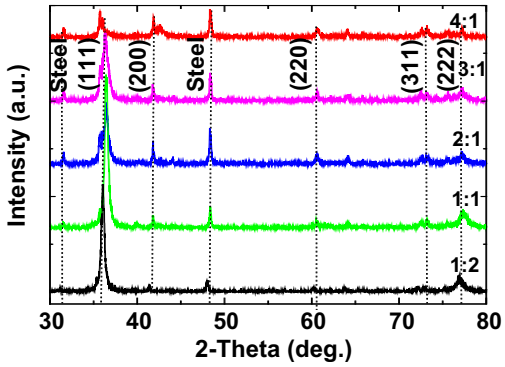

Fig. 3. XRD patterns for Ti–Si–N nanocomposite coatings deposited under various N_2/Ar ratios.

monotonically increased from 48.97 to 51.02 at. % with the increasing of N_2/Ar ratios from 0.5 to 4, while the Ti contents slightly decreased from 46.58 to 44.03 at %. The Si content in the resulting films was varied between 4.12 and 4.94 at. %. Because of the detecting limitation of EDX for light elements, more accurate experiments such as Rutherford Backscattering Spectrometry (RBS) have to be done. Fig. 4d shows a typical EDS spectrum for Ti–Si–N coatings deposited at N_2/Ar ratio of 3.

AFM was used to investigate the effect of N_2/Ar ratios on the surface roughness of the Ti–Si–N coatings and shown in Fig. 5. It is found that the surface became smoother and the root-mean-square (RMS) was gradually eliminated with increasing N_2/Ar ratios. No obvious microparticles were observed when N_2/Ar ratios reached above 2:1. This phenomenon can be attributed to the poisoning effect, namely, the Ti cathode was poisoned and a compound layer of TiN was formed on the target surface with increasing N_2/Ar ratios. TiN has a significantly higher melting (3150°) compared with the Ti cathode (1660°), which affects the plasma emission from arc spots, results in reduction in the number of Ti macroparticles in deposited Ti–Si–N coatings. Fig. 5d shows the cross-sectional micrograph for Ti–Si–N coatings deposited under typical conditions. Columnar structure was clearly seen and the coating revealed a dense nanostructure with a grain size of 10 nm. It was found that the Si addition into TiN coatings affected its microstructure to become finer in grain size and more random oriented in crystallographic direction [11]. The thickness of this sample is about 2.05 μm.

XPS was performed to investigate the bonding status in the Ti–Si–N coatings deposited under typical conditions and shown in Fig. 6. XPS general scan (Fig. 6a) of coatings showed the presence of Ti, Si, N and a very little amount of O. Si 2p peak with a binding energy of 101.6 eV was observed and shown in Fig. 6b. Peak position of Si 2p located at binding energy of 101.8 eV corresponding to N–Si bond of α-Si_3N_4 have been reported previously [12,13], which agreed well with the result of this study. Bonding status of Ti was also investigated and shown in Fig. 6c, peaks with binding energy of 455.8 and 461.4 eV were assigned to Ti $2p_{3/2}$ and $2p_{1/2}$ of stoichiometric TiN, respectively. Gaussian fitting of the N 1s spectrum (Fig. 6d) of the Ti–Si–N coating revealed typical features of TiN and Si_3N_4 with binding energies at 396.2 and 398.0 eV, respectively. Therefore, from XPS measurement, combined with our XRD results with no Si_3N_4 diffraction peaks, we concluded that Si_3N_4 was amorphous phase and Ti–Si–N coatings existed as nanocrystal-TiN/amorphous Si_3N_4, denoted as nc-TiN/a-Si_3N_4. The interface with TiN and Si_3N_4 is amorphous or crystalline [14,15]. High resolution cross-sectional TEM is demanded to distinguish the interface of the Ti–Si–N coatings.

A typical TEM image and selected area electron diffraction (SAED) pattern for the Ti–Si–N coatings deposited under typical conditions were shown in Fig. 7. The mean crystallite size was about 7–8 nm which in good agreement with our result obtained by XRD using Scherrer's formula [16]. The TiN crystallites were clearly distinguished from amorphous Si_3N_4 matrix by the lattice fringe

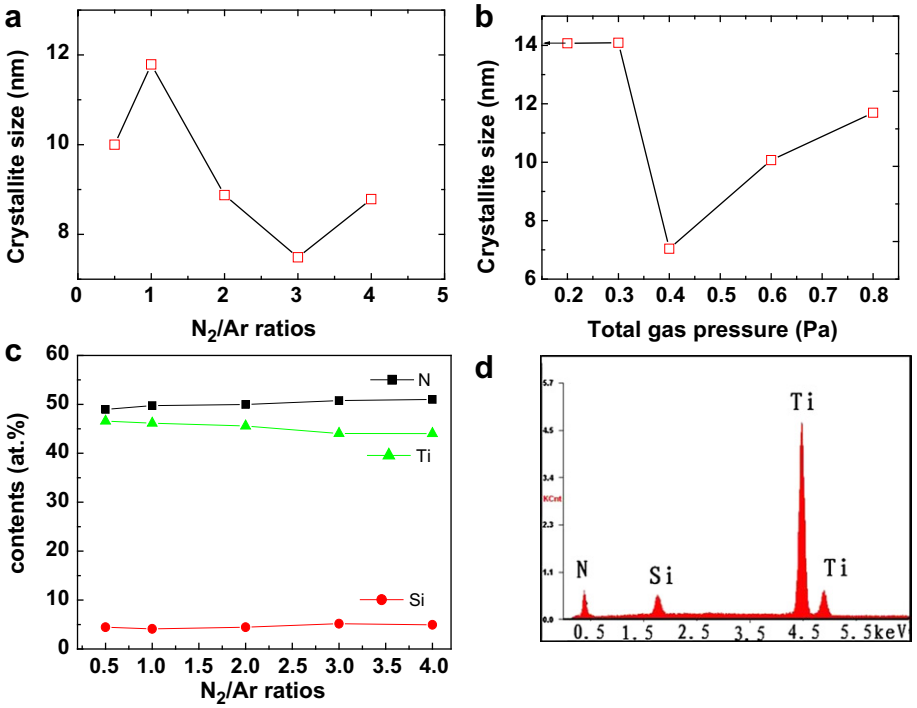

Fig. 4. TiN crystallite size calculated from XRD diffraction patterns of (111). (a) Under various N_2/Ar ratios. (b) Under various total gas pressure. (c) N, Ti, and Si contents in Ti–Si–N films as a function of N_2/Ar ratios at a fixed total gas pressure of 0.4 Pa (d) EDS spectrum for Ti–Si–N coatings deposited at N_2/Ar ratio of 3.

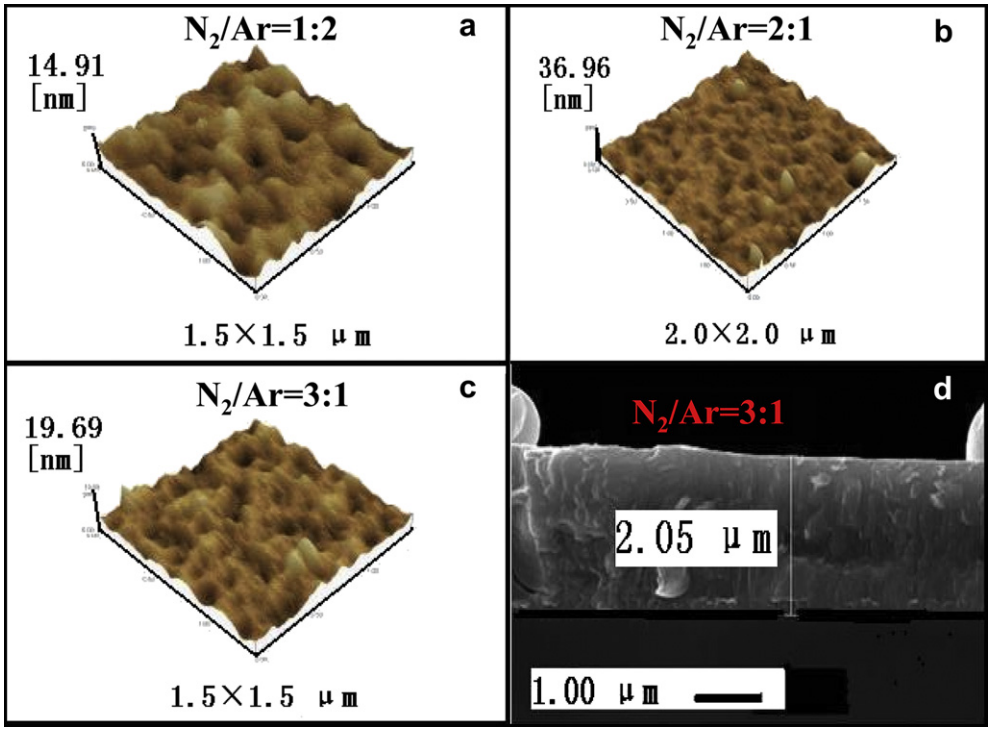

Fig. 5. XPS spectra for Ti–Si–N nanocomposite coatings deposited at typical conditions. (a) General scan, (b) Si 2p, (c) Ti 2p and (d) N 1s.

contrast, and finely embedded in amorphous Si_3N_4 matrix and randomly distributed across the whole region. The diffraction rings were originated from the crystallite TiN crystallites. The reason for formation of such nc-TiN/a-Si_3N_4 nanocomposite has been reported [2]. TiN phase can grow in high crystallinity at low temperature with the help of plasma energy. Nevertheless, Si_3N_4 crystallization required much high temperature due to high viscosity, so it was amorphous under the same experimental conditions [2]. Therefore, the structure of TiN crystallites embedded in an amorphous Si_3N_4 matrix can be also easily obtained using solid state target under mild synthesis conditions. In such structure, TiN crystallites would be almost ideally interconnected via the structurally flexible and strong Si_3N_4 matrix which can accommodate the coherency strain. When the structurally flexible and less polar Si_3N_4 wet the polar

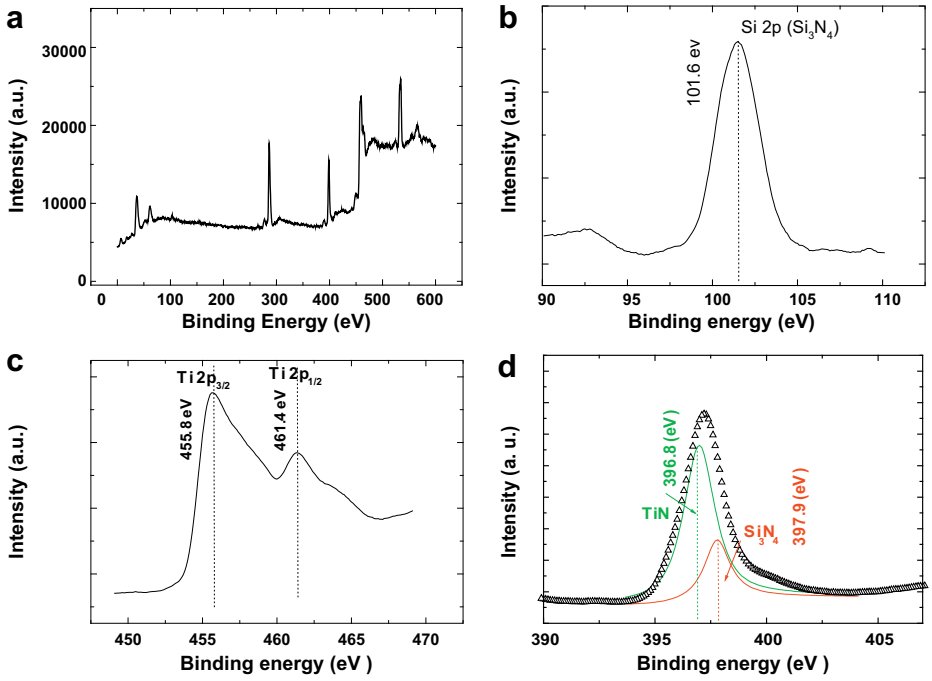

Fig. 6. AFM (a, b, c) and cross-sectional SEM (d) images for Ti–Si–N nanocomposite coatings deposited at various N_2/Ar ratios. (a) 1:1 (b) 2:1 (c) 3:1 and (d) 3:1.

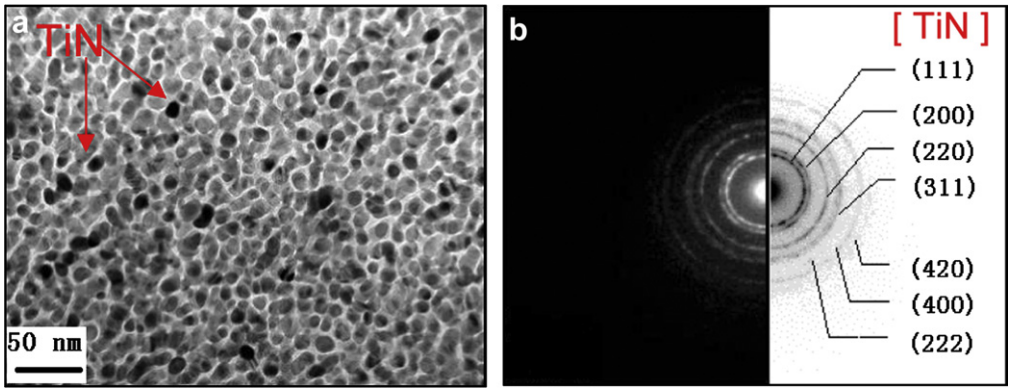

Fig. 7. Plan-view TEM and SAED images for Ti–Si–N nanocomposite coatings deposited at N_2/Ar ratio of 3:1.

surface of the TiN nanocrystals, the Gibbs free energy of the system will be decreased by the formation of a strong interface which has effects to limit grain-boundary sliding.

The hardness and friction coefficient of the Ti–Si–N coatings were measured by nano-indentation and ball-on-disc tester techniques and shown in Figs. 8 and 9, respectively. The nano-hardness increased steeply and reached the maximum value of approximately 58 GPa as the total gas pressure was increased from 0.2 to 0.4 Pa. The nano-hardness, however, reduced again when the gas pressure was further increased. At the same time, the maximum hardness was obtained when the N_2/Ar ratios was set at 3. Similar result has been obtained by using coupled plasma enhanced chemical vapor deposition with magnetic confinement method [2]. For friction coefficient, the values decreased gradually with increasing total gas pressure or N_2/Ar ratio. The reason may due to surface smoother and RMS eliminating as shown in AFM images. Many effects have been considered to explain the observed high harness of 58 GPa. These effects including smaller size of crystallite size, changes in preferred orientation, variation in the amorphous layer thickness, thermal mismatch between the layers, and existence of altering coherency strain fields from SiN_x layers with epitaxial interfaces to TiN [17]. In the case of hall-petch strengthening, hardness increases due to a reduction in grain size and thereby an increase in grain-boundary density which act as dislocation obstacles [17]. In our case, due to the small dimensions across the TiN nano-grains, nucleation and glide of dislocations is impeded, while the high cohesive strength of the thin inter-granular tissue phase inhibits grain-boundary sliding. Further work including TiN/SiN_x nano-multilayer and cross-sectional TEM experiments have to be done to study the effects of interfacial structure on the hardness.

The crystal quality is believed to be determined by two competing processes. First, the mean free path of the sputtered atoms could be reduced by the increase of total gas pressure, which result in a low kinetic energy and leads to a poor mobility when the atoms arrive at the substrate surface. This hinders nucleation and crystallization of the coatings. On the other hand, when the total gas is too low, the higher energy of the depositing atoms results in the re-sputtering of the deposition film. Therefore, an optimal pressure exists, e.g., 0.4 Pa in the present experiment. The pressure ratios of the N_2/Ar for the bombardment ion source have great influence on the quality of the Ti–Si–N coatings. N_2 is the essential element of the coatings and Ar can promote the ionization of the bombardment gas. The appropriate pressure ratio of N_2/Ar can be helpful to form the compound formality of Ti–Si–N coatings. The high hardness of the deposited Ti–Si–N coatings may be own to the plastic distortion [12] and dislocation blocking by the nanocrystalline structure [18]. The hardness value of Ti–Si–N coatings significantly increased up to 58 GPa for Ti–Si–N coatings deposited under typical conditions compared with that of ~30 GPa for TiN coatings [19]. This surprising enhanced hardness is believed to originate from the microstructure evolution TiN coatings with Si addition. In addition, grain-boundary hardening derived from the increased cohesive energy at inter phase boundaries along with the percolation phenomenon of amorphous phase is believed to play

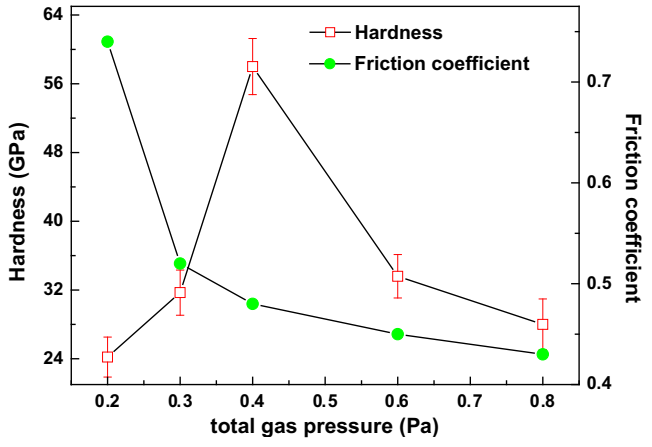

Fig. 8. Hardness and friction coefficient for Ti–Si–N nanocomposite coatings deposited at various total gas pressures.

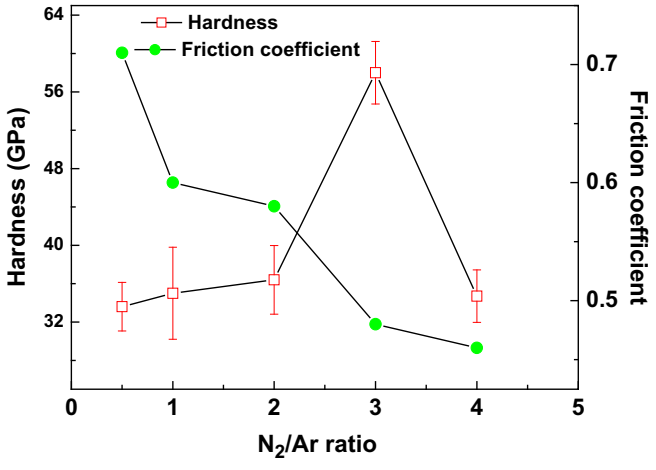

Fig. 9. Hardness and friction coefficient for Ti–Si–N nanocomposite coatings deposited at various N_2/Ar ratios.

a role in enhancing the hardness. On the other hand, the hardness decreased with a further increase in deposition pressure or N_2/Ar ratios after maximum hardness may due to the reduction in nanocomposite quality. Interface structure in super-hard TiN–SiN nanolaminates and nanocomposites had been studied by L. Hultman et al. [15,20]. Their results on the growth of SiN_x/TiN nanolaminates on MgO (001) show that the SiN_x layers are initially epitaxial c-SiN prior to reaching an epitaxial breakdown thickness, beyond which the SiN_x layers become amorphous. They attribute the epitaxial stabilization of metastable cubic SiN on TiN (001) to pseudomorphic forces. However, the corresponding interfacial strain increases linearly with SiN_x and as above the breakdown thickness, the strain energy becomes sufficiently large that the epitaxial growth front breaks down.

Also, in these Ti–Si–N nanocomposite coatings, TiN crystallites with a smaller size may be almost perfectly embedded in a structurally flexible and strong Si_3N_4 matrix. Dislocation can't form in the so small TiN crystallites and the formation of cracks in the Si_3N_4 is hindered due to its three dimensional skeleton structure, which provides complex boundaries to accommodate coherent strain effect and grain boundaries strengthening effect. So, maximum hardness would be obtained with smaller crystallites sizes which agree well with our case, the minimum crystallite size was obtained when total gas pressure and N_2/Ar ratio were set at 0.4 Pa and 3:1, respectively. The crystallite size and preferred orientation, which can be tailored by adjustment of N_2/Ar ratio, decide the mechanical properties of Ti–Si–N coatings [5].

4. Conclusions

TiN-containing amorphous Ti–Si–N nanocomposite coatings were deposited by using a modified closed field unbalanced magnetron sputtering system which is arc assisted and consists of two circles of targets. The coatings exhibit good mechanical properties that are greatly influenced by the total gas pressure and N_2/Ar ratios. Coatings deposited under optimum conditions exhibits excellent performance with a low friction coefficient of 0.42 and a high hardness of 58 GPa. These properties make it possible for industrial applications.

Acknowledgments

This work was supported by national Natural Science Foundation of China under contract 10435060 and 10675095 and by SRF for ROCS, State Education Ministry.

References

[1] Niederhofer A, Nesladek P, Mannling HD, Moto K, Veprek S, Jilek M. Surf Coat Technol 1999;120:173.
[2] Zhao HY, Fan QL, Song LX, Zhang T, Shi EW, Hu XF. Appl Surf Sci 2006;252:3065.
[3] Kang MC, Kim JS, Kim KH. Surf Coat Technol 2005;200:1939.
[4] Jeon JH, Choi SR, Chung WS, Kim KH. Surf Coat Technol 2004;188:415.
[5] Veprek S, Reiprich S, Li S. Appl Phys Lett 1995;66:2640.
[6] Flink A, Larsson T, Sjolen J, Karlsson L, Hultman L. Surf Coat Technol 2005;200:1535.
[7] Mei FH, Shao N, Hu XP, Li GY, Gu MY. Mater Lett 2005;59:2442.
[8] Li ZG, Mori M, Miyake S, Kumagai M, Saito H, Muramatsu Y. Surf Coat Technol 2005;193:345.
[9] Diserens M, Patscheider J, Levy F. Surf Coat Technol 1998;108:241.
[10] Kim KH, Choi SR, Yoon SY. Surf Coat Technol 2002;298:243.
[11] Pilloud D, Pierson JF, Steyer P, Mege A, Stauder B, Jacquot P. Mater Lett 2007;61:2506.
[12] Nose M, Deguchi Y, Mae T, Honbo E, Nagae T, Nogi K. Surf Coat Technol 2003;174:261.
[13] Du H, Tressler RE, Spear KE, Pantano CG. J Electronchem Soc 1989;136:1527.
[14] Flink A, Beckers M, Sjolen J, Larsson T, Braun S, Karlsson L, et al. J Mater Res 2009;24:2483.
[15] Hultman L, Bareno J, Flink A, Soderberg H, Larsson K, Perova V, et al. Phys Rev B 2007;75:155437.
[16] Christiansen S, Albrecht M, Strunk HP, Veprek S. J Vac Sci Technol B 1998;16:19.
[17] Soderberg H, Oden M, Molina-Aldareguia JM, Hultman L. J Appl Phys 2005;97:114327.
[18] Zhang S, Sun D, Fu YQ, Du HJ. Surf Coat Technol 2003;167:113.
[19] Steyer P, Mege A, Pech D, Mendibide C, Fontaine J, Pierson JF, et al. Surf Coat Technol 2008;202:2268.
[20] Alling B, Isaev EI, Flink A, Hultman L, Abrikosov IA. Phys Rev B 2008;78:132103.